ISSN: 2690-909X

Research Article

Advances in Neurology and Neuroscience

TTR Exon-Humanized Mice as a Model for Genotype-Dependent Transthyretin Deposition: Supportive Evidence for RBP4 as a Natural Stabilizer

Zhenghua Li[1,2], Hideki Kanazashi[3], Yuya Murakami[3], Rie Fujikawa[3], Naoko Matsushita[3], Toru Takeo[1], Aki Sugano[4], Mika Ohta[5], Yutaka Takaoka[5] and Kenichi Yamamura[1,2*]

[1]*Institute of Resource Development and Analysis, Kumamoto University, Kumamoto, Japan*

[2]*Transgenic Group, Inc., Fukuoka, Japan*

[3]*Transgenic, Inc., Kobe, Japan*

[4]*Graduate School of Medicine and Pharmaceutical Sciences, University of Toyama, Toyama, Japan*

[5]*Division of Medical Informatics and Bioinformatics, Kobe University Hospital, Kobe, Japan*

***Corresponding Author**
Kenichi Yamamura, Institute of Resource Development and Analysis, Kumamoto University, Kumamoto, Japan.

Submitted: 2026, July 09 **Accepted:** 2026, Aug 10; **Published:** 2026, Aug 19

Citation: Li, Z., Kanazashi, H., Murakami, Y., Fujikawa, R., Matsushita, N., et. al.(2026). TTR Exon-Humanized Mice as a Model for Genotype-Dependent Transthyretin Deposition: Supportive Evidence for RBP4 as a Natural Stabilizer. *Adv Neur Sci, 9*(3), 01-17.

Abstract

Transthyretin amyloidosis is caused by destabilization, dissociation, and tissue deposition of transthyretin (TTR). Although several transgenic and knock-in mouse models have been generated, many models are limited by non-physiological copy number, low expression, or the formation of hybrid tetramers between mouse and human TTR. We previously generated TTR exon-humanized mice in which mouse Ttr exons were replaced with corresponding human TTR exons while preserving the mouse genomic structure. In the present study, we introduced the Val30Met mutation into the TTR exon-humanized allele and generated three genotypes: TtrhTTRV30e/hTTRV30e, TtrhTTRM30e/hTTRM30e, and TtrhTTRV30e/hTTRM30e mice. We examined non-fibrillar human TTR deposition by immunohistochemistry in ileum, kidney, and sciatic nerve at 26 and 52 weeks of age, using a semi-quantitative scoring system. Genotype-dependent TTR deposition was observed in multiple tissues. TTR deposition was prominent in V30/V30 and V30/M30 mice, whereas M30/M30 mice consistently showed lower deposition scores. Notably, TTR-positive deposits were detected in the sciatic nerve at 52 weeks of age. Direct fast scarlet staining did not detect amyloid fibrils, indicating that the observed deposits represented non-fibrillar or pre-amyloid TTR deposition. Serum human TTR levels showed modest genotype-dependent differences, whereas serum mouse RBP4 levels differed markedly among genotypes. Supportive computer simulation analysis suggested that the predicted binding stability between mouse RBP4 and TTR was highest for mouse TTR, intermediate for human TTR Met30, and lowest for human TTR Val30. These findings indicate that TTR exon-humanized mice provide a useful model for evaluating genotype-dependent TTR deposition and support the possibility that RBP4 functions as a natural stabilizer of circulating TTR.

Keywords: Transthyretin, TTR, RBP4, Exon-Humanized Mouse, Val30Met, Amyloid, Non-Fibrillar Deposition, Sciatic Nerve

1. Introduction

Transthyretin (TTR) is a tetrameric plasma protein primarily synthesized in the liver and choroid plexus [1-15]. It functions as a carrier protein for thyroxine and retinol-binding protein 4 (RBP4) [16,17]. The TTR tetramer is normally stable in circulation, however, tetramer dissociation is considered a critical early step in TTR amyloidogenesis [4,5]. After dissociation, partially unfolded monomers can form non-fibrillar aggregates,

protofibrils, and mature amyloid fibrils. Pathogenic variants of TTR cause hereditary transthyretin amyloidosis, historically known as familial amyloid polyneuropathy, whereas wild-type TTR can also form amyloid deposits in aging individuals [1-3]. Among TTR variants, Val30Met is one of the best-characterized mutations associated with hereditary amyloid polyneuropathy [2,3,8-10]. Most patients are heterozygous for the Val30Met mutation. Interestingly, homozygous Val30Met patients are rare and are not necessarily more severely affected than heterozygous patients. This observation suggests that the relationship between TTR genotype and tissue deposition is not simply determined by the number of mutant alleles, but may depend on tetramer composition, molecular stability, and interactions with other serum proteins.

Mouse models are essential for investigating TTR amyloidogenesis and for evaluating new therapeutic strategies. Several transgenic mouse models expressing human TTR variants have been generated [8-11,18,19]. However, conventional transgenic models have important limitations, including non-physiological transgene copy number, ectopic or variable expression, and the continued presence of endogenous mouse TTR [6,12]. Because TTR forms tetramers, mouse TTR can associate with human TTR and generate hybrid tetramers that are more stable than human TTR homotetramers [6,7]. This may interfere with the analysis of amyloid formation and the evaluation of TTR stabilizers or gene therapies.

To overcome these limitations, we previously generated TTR exon-humanized mice in which the mouse Ttr coding exons were replaced by the corresponding human TTR exons while preserving mouse intronic and regulatory sequences [15]. These mice showed physiological tissue specificity and serum TTR expression, suggesting that the preservation of the genomic context is important for quantitative and spatially appropriate TTR expression. This model is expected to be particularly useful for testing therapies that directly target the human TTR sequence while maintaining physiological regulation of the Ttr locus.

RBP4 may also influence TTR amyloidogenesis. In plasma, RBP4 circulates in complex with TTR, and this interaction prevents the glomerular filtration of RBP4 [14,17]. Conversely, binding to RBP4 may stabilize TTR in circulation [16]. Previous studies using mice humanized at both the Ttr and Rbp4 loci suggested that the stability of the TTR-RBP4 complex influences TTR deposition. Therefore, the interaction between TTR and RBP4 may be an important determinant of circulating TTR stability and tissue deposition. In the present study, we generated TTR exon-humanized mice carrying the Val30Met mutation by introducing the Met30 codon into the previously established humanized Val30 TTR exon allele. By crossing these mice, we obtained V30/V30, M30/M30, and V30/M30 mice. We then analyzed tissue TTR deposition in ileum, kidney, and sciatic nerve at 26 and 52 weeks of age using anti-human TTR immunohistochemistry and a semi-quantitative scoring system. In addition, we examined serum human TTR and mouse RBP4 levels and performed supportive computer simulation analysis of TTR-RBP4 binding stability. Our findings demonstrate that TTR exon-humanized mice reveal genotype-dependent, non-fibrillar TTR deposition and provide supportive evidence that RBP4 may function as a natural stabilizer of circulating TTR.

2. Materials and Methods

2.1. Animals

TTR exon-humanized mice carrying human TTR Val30 exons, TtrhTTRV30e/hTTRV30e, were previously generated by replacing mouse Ttr exons with corresponding human TTR exons while retaining the mouse intronic and regulatory regions [15]. In the present study, TtrhTTRM30e/hTTRM30e mice were generated by introducing the Val30Met mutation into the TtrhTTRV30e allele. TtrhTTRV30e/hTTRV30e mice are hereafter referred to as V30/V30 mice, TtrhTTRM30e/hTTRM30e mice as M30/M30 mice, and TtrhTTRV30e/hTTRM30e mice as V30/M30 mice. Only male mice were used for the main analyses to avoid potential confounding by sex-related differences in body weight and serum RBP4 levels. Mice were analyzed at 26 and 52 weeks of age. All animal experiments were performed in accordance with institutional guidelines and approved protocols.

2.2. Generation of $Ttr^{hTTRM30e}$ mice

The $Ttr^{hTTRM30e}$ allele was generated from fertilized eggs of $Ttr^{hTTRV30e}$ mice by genome editing. A guide RNA targeting the humanized TTR exon 2 region was selected, and donor single-stranded oligodeoxynucleotide DNA containing the Val30Met mutation was introduced together with CRISPR-Cas9 components by microinjection. The Val30 codon GTG was replaced with the Met30 codon ATG. Founder mice carrying the targeted mutation without additional mutations were selected and bred to establish the $Ttr^{hTTRM30e}$ line. V30/V30, M30/M30, and V30/M30 mice were generated by intercrossing the respective strains.

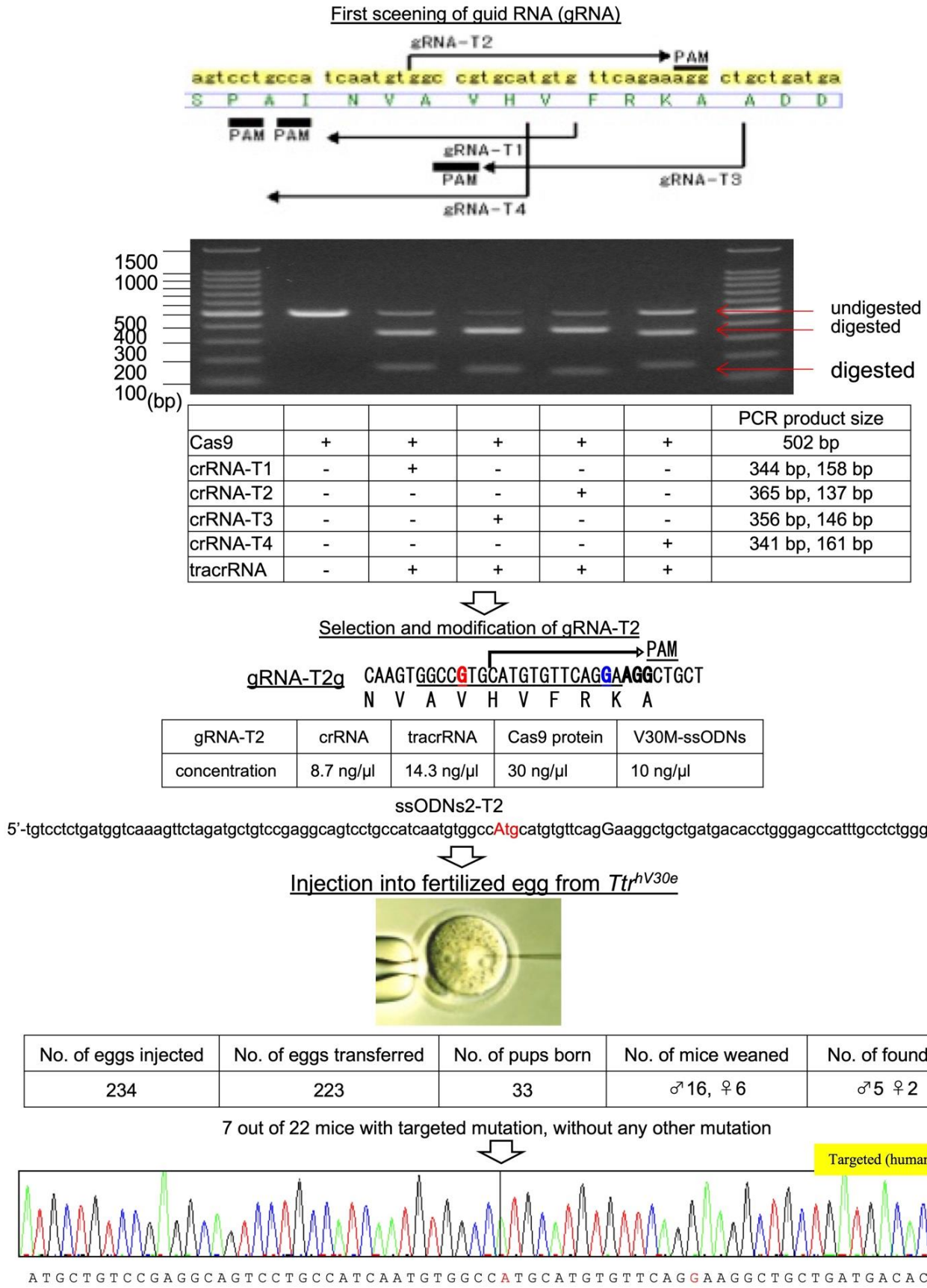

						PCR product size
Cas9	+	+	+	+	+	502 bp
crRNA-T1	-	+	-	-	-	344 bp, 158 bp
crRNA-T2	-	-	-	+	-	365 bp, 137 bp
crRNA-T3	-	-	+	-	-	356 bp, 146 bp
crRNA-T4	-	-	-	-	+	341 bp, 161 bp
tracrRNA	-	+	+	+	+	

gRNA-T2	crRNA	tracrRNA	Cas9 protein	V30M-ssODNs
concentration	8.7 ng/μl	14.3 ng/μl	30 ng/μl	10 ng/μl

ssODNs2-T2

5'-tgtcctctgatggtcaaagttctagatgctgtccgaggcagtcctgccatcaatgtggccAtgcatgtgttcagGaaggctgctgatgacacctgggagccatttgcctctgggtaagctt-3'

No. of eggs injected	No. of eggs transferred	No. of pups born	No. of mice weaned	No. of founder
234	223	33	♂16, ♀6	♂5 ♀2

Figure 1: Production of TTR Exon-Humanized Mice Carrying the Val30Met Mutation

The Val30Met mutation was introduced into the previously generated Ttr^hTTRV30e allele by CRISPR-Cas9-mediated genome editing. A guide RNA targeting the humanized TTR exon 2 region and donor single-stranded oligodeoxynucleotide DNA were introduced into fertilized eggs from Ttr^hTTRV30e mice. The Val30 codon GTG was replaced with the Met30 codon ATG. Founder mice carrying the targeted mutation without additional mutations were selected and used to establish the Ttr^hTTRM30e line.

2.3. Genotyping

Genotypes of $Tt^{rhTTRV30e}$ and $Ttr^{hTTRM30e}$ alleles were determined by PCR-RFLP analysis. A genomic region containing exon 2 was amplified using the primers ex2-GXXFP-F1 and ex2-GXXFP-R2. The PCR product size was 502 bp. The M30 allele contains a restriction site introduced by the Val30Met substitution, and digestion allowed discrimination among V30/V30, V30/M30, and M30/M30 genotypes. V30/V30 mice showed an undigested 502-bp band, M30/M30 mice showed digested fragments of 350 bp and 152 bp, and V30/M30 mice showed all three bands.

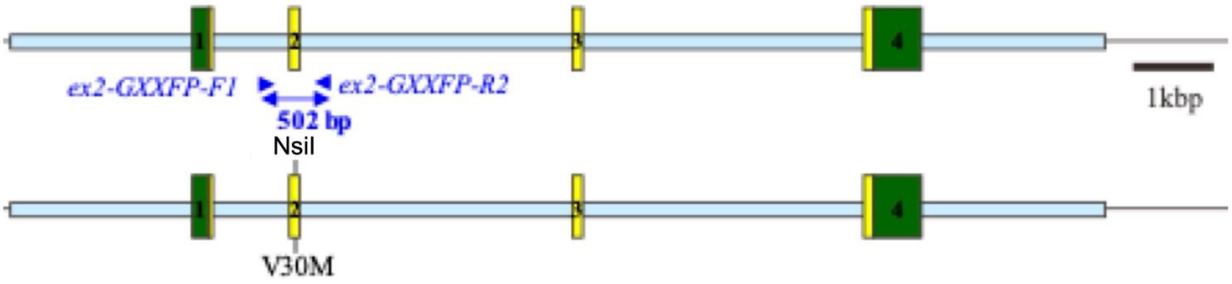

Ttr<hTTRV30e>とTtr<hTTRM30e>の判別のGenotyping PCR-RFLP解析条件				
PCR primers	Primer name	Primer sequence		Length
	ex2-GXXFP-F1	ATGGCTCTCAGAGGGCCTATTTTC		24
	ex2-GXXFP-R2	CCCTCTAGCTGGTAAGTTGTGTG		23
PCR conditions	PCR enzyme	PrimeSTAR GXL (TaKaRa Bio)		
	Thermocycler	GeneAmp PCR System 9700 (Applied Bio Systems)		
	Component / Volume	Cycling condition	3 -step	
	template 1.0 µl	Predenature : 94.0 ℃	2 min.	
	5 × GXL buffer 5.0 µl	Denature : 98.0 ℃	10 sec.	
	2.5 mM dNTPs each 2.0 µl	Annealing : 65.0 ℃	15 sec.	
	Forward primer (10 µM) 0.75 µl	Extension : 68.0 ℃	1 min.	
	Reverse primer (10 µM) 0.75 µl	Final extension : 68.0 ℃	1 min.	
	PrimeSTAR GXL 0.5 µl	Hold : 4.0 ℃	∞	
	ddw 15.0 µl	※Number of cycles		30 cycles
	Total 25.0 µl	Size of PCR product :		502 bp
		Size of PCR product (*Msc*I digested) :		350 bp ,152 bp

Example (Ttr<hV30/hM30>xTtr<hv30xhM30>)F2

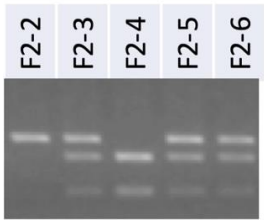

	Band size	Genotype
F2-1	502 bp	Ttr<hV30e/hV30e>
F2-2	502 bp, 350 bp, 152 bp	Ttr<hV30e/hM30e>
F2-3	350 bp, 152 bp	Ttr<hM30e/hM30e>
F2-4	502 bp, 350 bp, 152 bp	Ttr<hV30e/hM30e>
F2-5	502 bp, 350 bp, 152 bp	Ttr<hV30e/hM30e>

Figure 2: Genotyping of $Ttr^{hTTRV30e}$ and $Ttr^{hTTRM30e}$ mice

Genotypes were determined by PCR-RFLP analysis. A 502-bp PCR product containing the Val30Met site was amplified. V30/V30 mice showed an undigested 502-bp band, M30/M30 mice showed digested 350-bp and 152-bp fragments, and V30/M30 mice showed all three bands.

2.4. Body Weight Measurement

Body weight was measured in male V30/V30, M30/M30, and V30/M30 mice at 26 and 52 weeks of age. Body weight was used as a general indicator of health and to determine whether genotype had a major effect on growth or systemic condition.

2.5. Tissue Preparation

Male mice were sacrificed at 26 or 52 weeks of age. Tissues including ileum, kidney, and sciatic nerve were excised, fixed in neutral-buffered formalin, embedded in paraffin, and sectioned for histological and immunohistochemical analyses.

2.6. Immunohistochemistry for Human TTR

Immunohistochemistry was performed using paraffin sections. Sections were deparaffinized, and antigen retrieval was performed using HistoVT One. Endogenous peroxidase activity was blocked, followed by blocking of non-specific secondary antibody binding. Sections were incubated overnight at 4°C with anti-human TTR antibody. Amplifier antibody and polymer reagent were then applied, and the signal was visualized using DAB substrate. Sections were counterstained with Mayer's hematoxylin, dehydrated, cleared, and mounted. The immunohistochemical staining protocol was based on the ImmPRESS Excel Amplified Anti-Rabbit IgG Staining Kit. Anti-human TTR antibody was used at a dilution of approximately 1:1000 to 1:1500.

Table 1. Immunohistochemical condition

ImmPRESS® Excel Amplified Anti-Rabbit IgG Staining Kit（Vector #MP-7601） was used for immunohistchemistry

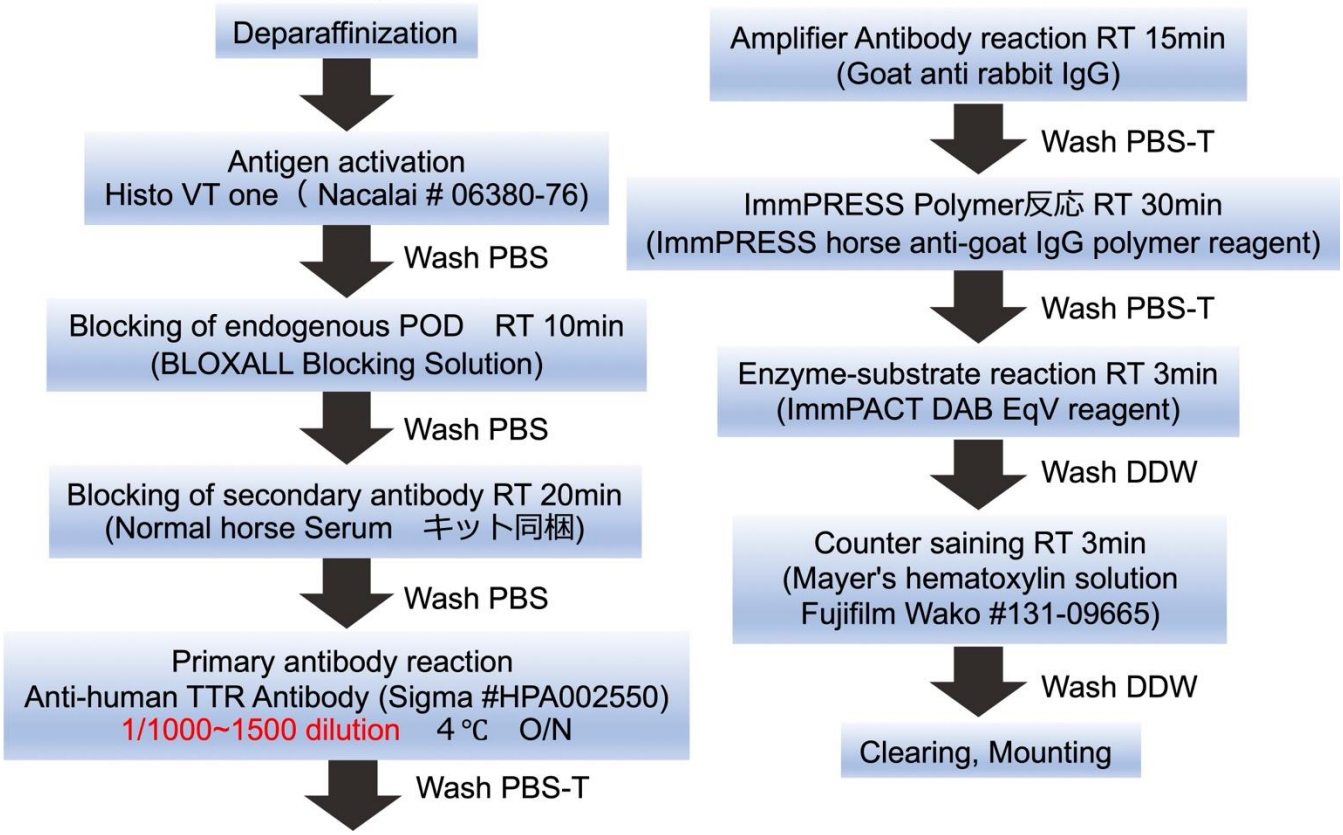

Table 2. Score of hTTR deposition

A. 26 weeks of age

	hTTR IHC score					
	Male 26w					
	Ileum			Kidney		
Mouse No.	V/V	M/M	V/M	V/V	M/M	V/M
1	3	0.5	3	3	0.5	3
2	2	0.5	3	3	0.5	3
3	3	0.5	2	3	0.5	2
4	3	0.5	3	3	0.5	3
5	2	0.5	2	3	0.5	2
6	3	1	3	2	0.5	2
7	3	2	2	3	1	2
8	3	0.5	3	2	0.5	3
9	3	1	1	2	1	3
10	3	0.5	0.5	2	0.5	2
11	3	1	1	3	0.5	2
12	2	0.5	0.5	3	0.5	3
13	3	0.5	0.5	3	0.5	2
14	3	0.5	0.5	3	0.5	3
15	3	1	1	3	0.5	2
SUM	42	11	25.5	41	8.5	37
Average	2.80	0.73	1.70	2.73	0.57	2.47
STDEVP	0.400	0.403	1.061	0.442	0.170	0.499
	p<0.001			p<0.001		
	p=0.002			p=0.071		
		p=0.003			p<0.001	

B. 52 weeks of age

	hTTR IHC score								
	Male 52w								
	Ileum			Kidney			Sciatic N		
Mouse No.	V/V	M/M	V/M	V/V	M/M	V/M	V/V	M/M	V/M
16	3	0.5	2	3	0.5	3	2	0.5	1
17	3	0.5	2	3	0.5	3	2	0.5	1
18	0.5	1	2	3	1	3	1	0.5	1
19	2	1	3	3	0.5	3	3	0.5	0.5
20	3	0.5	3	3	1	3	3	1	0.5
21	3	0.5	2	3	1	3	3	0.5	1
22	3	1	2	3	0.5	3	2	0.5	1
23	3	1	3	3	0.5	3	3	1	1
24	3	2	2	3	0.5	1	0.5	1	1
25	3	1	3	3	0.5	3	1	0.5	0.5
30	3	1	3	3	1	3	2	1	0.5
27	3	2	3	3	0.5	3	0.5	0.5	0.5
28	2	1	3	2	0.5	3	0.5	0.5	0.5
29	3	1	2	3	0.5	3	1	1	1
30	3	1	3	3	1	3	0.5	0.5	1
SUM	40.5	15	38	44	10	43	25	10	12
Average	2.70	1.00	2.53	2.93	0.67	2.87	1.67	0.67	0.80
STDEVP	0.678	0.447	0.499	0.249	0.236	0.499	0.978	0.236	0.245
	p<0.001			p<0.001			p=0.002		
	p=0.091			p=0.481			p=0.013		
		p<0.001			p<0.001			p=0.075	

2.7. Semi-Quantitative Scoring of TTR Deposition

Because TTR-positive deposits were widely distributed and differed by tissue, quantitative image analysis using ImageJ was considered inappropriate. Instead, TTR deposition was evaluated using tissue-specific pathological criteria based on immunohistochemical staining intensity and distribution.

For statistical analysis, TTR deposition was converted into a semi-quantitative score as follows: no staining, 0, trace or ± staining, 0.5, mild or + staining, 1, moderate or ++ staining, 2, and marked or +++ staining, 3. In ileum, ± staining was defined as positive signals restricted to blood vessels and perivascular areas. + staining indicated positive signals in the perivascular region, lamina propria, muscularis layer, and serosa occupying 30% or less of the section. ++ staining indicated positive signals occupying approximately 30–70% of the section. +++ staining indicated extensive positive signals occupying 70% or more of the section.

In kidney, ± staining was defined as positive signals limited mainly to glomeruli. + staining indicated clear positive signals in glomeruli and proximal tubules. ++ staining indicated more extensive positive signals in glomeruli and proximal tubules, with additional signals in the medullary region. +++ staining indicated strong and widespread positive signals, particularly in proximal tubules and the medullary region. In sciatic nerve, scoring criteria were modified because even small amounts of deposition in nerve parenchyma were considered biologically important. ± staining indicated a small number of positive signals in the perineurium, endoneurium, or nerve fibers. + and ++ indicated increasing numbers of positive deposits, and +++ indicated multiple areas with more extensive deposition.

2.8. Direct Fast Scarlet Staining

To determine whether TTR-positive deposits represented mature amyloid fibrils, serial sections were stained with Direct fast scarlet. Sections were examined under bright-field and polarized light microscopy. Amyloid fibril deposition was assessed by the presence of characteristic birefringence under polarized light.

2.9. ELISA Assays

Serum human TTR and mouse RBP4 concentrations were measured using commercial ELISA kits according to the manufacturers' instructions. Human TTR was measured using a human TTR ELISA kit (KA0495, Abnova, Taipei, China), and mouse RBP4 was measured using a mouse RBP4 ELISA kit (Mouse Retinol-Binding protein 4 ELISA Kit SimpleStep, ab202404, Abcam, Tokyo, Japan). Serum was collected from male mice at the indicated ages.

2.10. Computational Analysis of TTR-RBP4 Binding Stability

Computational analysis was performed as supportive evidence to evaluate whether different TTR tetramers differ in their binding stability with mouse RBP4 complexed with retinol. Structural models of mouse TTR, human wild-type TTR Val30, and human TTR Val30Met tetramers were prepared. The mouse RBP4-retinol complex was modeled and docked to each TTR tetramer. After selection of appropriate TTR-RBP4-retinol complex structures, the models were subjected to molecular mechanics/molecular dynamics refinement. Structural convergence was assessed by RMSD analysis, and the stereochemical quality of the modeled structures was evaluated by Ramachandran plot analysis. Binding free energy between each TTR tetramer and mouse RBP4-retinol was then calculated using the gmx_MMPBSA program. Calculated binding free energy values are expressed as kcal/mol. More negative binding free energy values were interpreted as indicating more stable binding between TTR and RBP4-retinol. Because this analysis was performed to provide supportive mechanistic information, the computational results were interpreted in relation to the serum RBP4 data and tissue TTR deposition patterns.

2.11. Statistical Analysis

Data are presented as mean ± SEM unless otherwise indicated. TTR deposition scores were treated as semi-quantitative ordinal data. Comparisons between two groups were performed using the Mann-Whitney U test. For comparisons among three genotypes, the Kruskal-Wallis test was used, followed by pairwise Mann-Whitney U tests when appropriate. A p value <0.05 was considered statistically significant.

3. Results

3.1. Generation of $Ttr^{hTTRM30e}$ mice from $Ttr^{hTTRV30e}$ mice (Figure 1)

We previously generated TTR exon-humanized mice in which mouse Ttr exons were replaced with human TTR Val30 exons. To generate an exon-humanized model carrying the Val30Met mutation, CRISPR-Cas9-mediated genome editing was performed in fertilized eggs obtained from V30/V30 mice. The Val30 codon GTG was replaced with the Met30 codon ATG. Among the mice obtained, targeted mice carrying the desired Val30Met mutation without additional mutations were selected. The resulting V30/M30 mice were crossed to establish the M30/M30 line.

By crossing V30 and M30 lines, three genotypes were generated for analysis: V30/V30, M30/M30, and V30/M30 mice.

3.2. Genotyping of V30/V30, M30/M30, and V30/M30 mice (Figure 2)

PCR-RFLP analysis was used to distinguish the V30 and M30 alleles. Amplification of the exon 2-containing region yielded a 502-bp PCR product. Restriction enzyme digestion allowed discrimination of the M30 allele. V30/V30 mice showed the undigested 502-bp band, M30/M30 mice showed 350-bp and 152-bp fragments, and V30/M30 mice showed the combined pattern. This genotyping method enabled reliable identification of the three genotypes used in subsequent analyses.

3.3. Body Weight and General Condition

Body weight was measured at 26 and 52 weeks of age. At 26 weeks, V30/V30 mice showed slightly higher body weight than M30/M30 and V30/M30 mice. However, no major genotype-dependent difference in body weight was observed at 52 weeks of age. These results indicate that the three genotypes were generally comparable in overall growth and systemic condition at the ages analyzed.

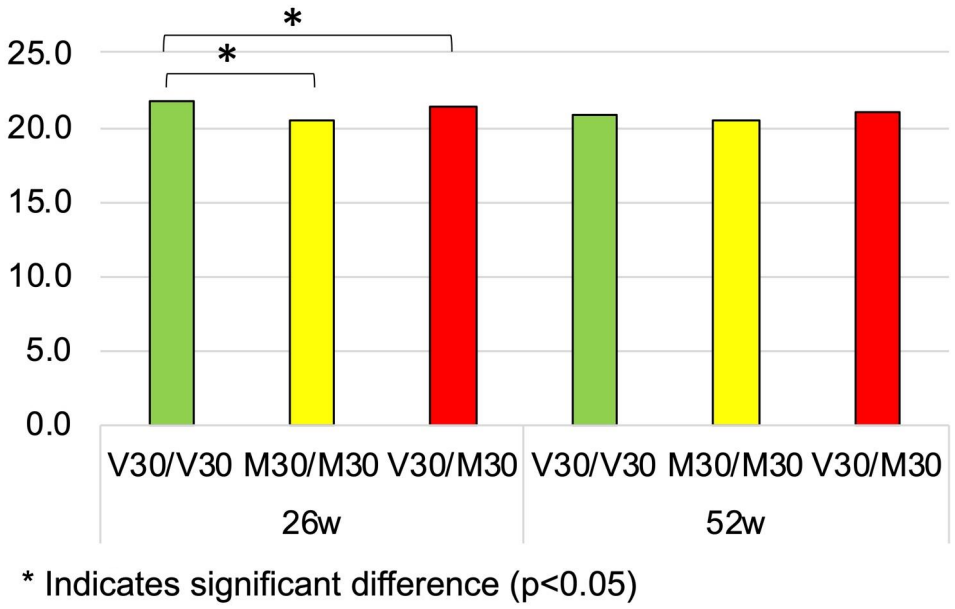

Figure 3: Body Weight

Body weight was measured in male V30/V30, M30/M30, and V30/M30 mice at 26 and 52 weeks of age. Although V30/V30 mice showed slightly higher body weight at 26 weeks of age, no major genotype-dependent difference was observed at 52 weeks. Asterisks indicate significant differences.

3.4. Establishment of a Semi-Quantitative Scoring System for non-fibrillar hTTR Deposition

Anti-human TTR immunohistochemistry revealed unexpectedly widespread TTR-positive deposits in several tissues. Because the distribution of staining differed among tissues and was not suitable for simple area-based image quantification, we established tissue-specific scoring criteria for ileum, kidney, and sciatic nerve. Staining was classified into five categories: negative, ±, +, ++, and +++, corresponding to numerical scores of 0, 0.5, 1, 2, and 3, respectively. This approach allowed semi-quantitative evaluation of TTR deposition, rather than simply recording the number of mice with positive staining. The scoring system was then applied to all samples used for genotype- and age-dependent analyses.

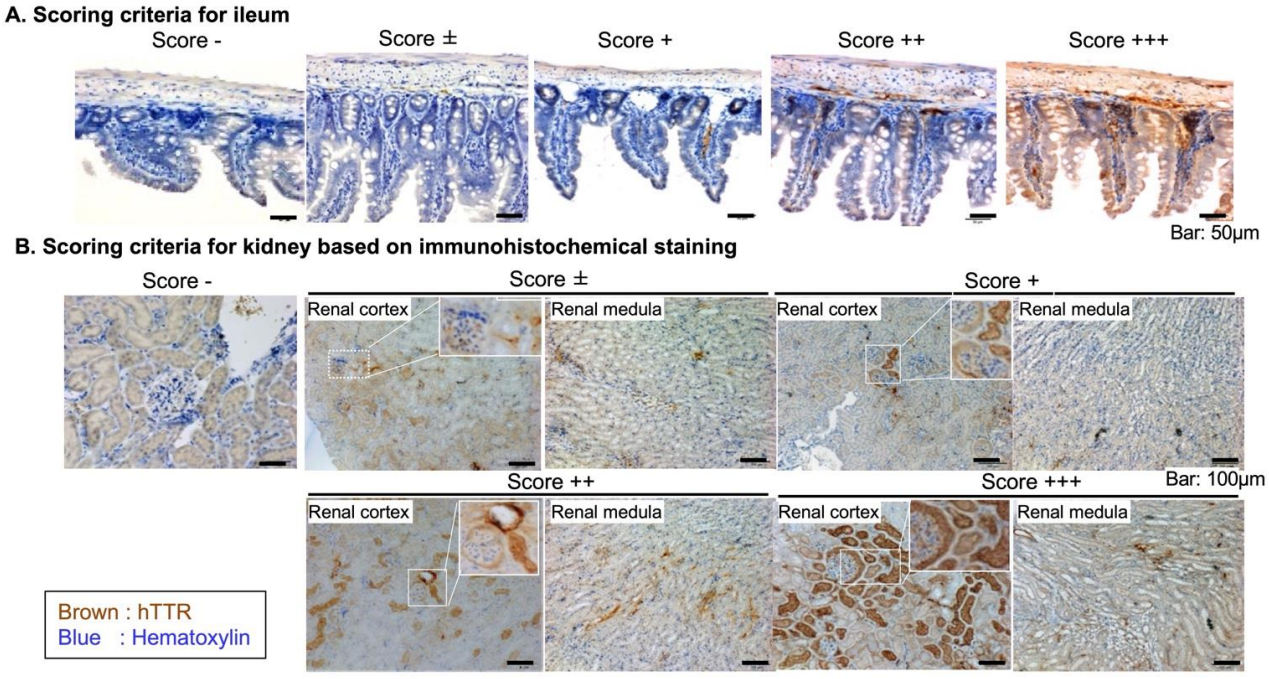

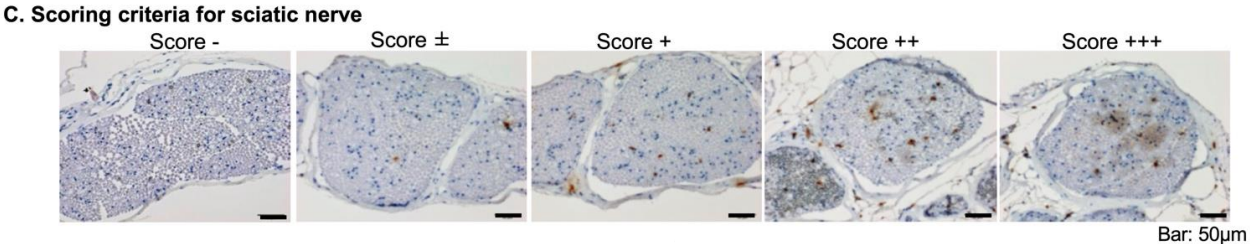

Figure 4: Scoring Criteria for hTTR Deposition based on Immunohistochemical Staining

TTR deposition was scored separately in ileum, kidney, and sciatic nerve according to tissue-specific criteria. Staining was classified as negative, ±, +, ++, or +++, and converted into numerical scores of 0, 0.5, 1, 2, and 3, respectively. Representative images for each score are shown.

3.5. Genotype-Dependent hTTR Deposition in ileum

At 26 weeks of age, TTR deposition in ileum differed significantly among the three genotypes. V30/V30 and V30/M30 mice showed extensive TTR-positive staining, whereas M30/M30 mice showed only minimal deposition. The mean deposition scores were 2.60 ± 0.24 in V30/V30 mice, 0.50 ± 0.00 in M30/M30 mice, and 2.60 ± 0.24 in V30/M30 mice. Kruskal–Wallis analysis showed a significant genotype effect. Pairwise comparisons showed that M30/M30 mice had significantly lower deposition scores than both V30/V30 and V30/M30 mice, whereas no significant difference was observed between V30/V30 and V30/M30 mice. At 52 weeks of age, ileal TTR deposition remained genotype-dependent. V30/V30 and V30/M30 mice showed relatively high deposition scores, whereas M30/M30 mice showed lower scores. The mean deposition scores were 2.30 ± 0.49 in V30/V30 mice, 0.70 ± 0.12 in M30/M30 mice, and 2.40 ± 0.24 in V30/M30 mice. The genotype effect remained significant, with M30/M30 mice showing significantly lower deposition than V30/M30 mice. These results indicate that genotype-dependent TTR deposition is already evident in the ileum by 26 weeks of age and persists at 52 weeks.

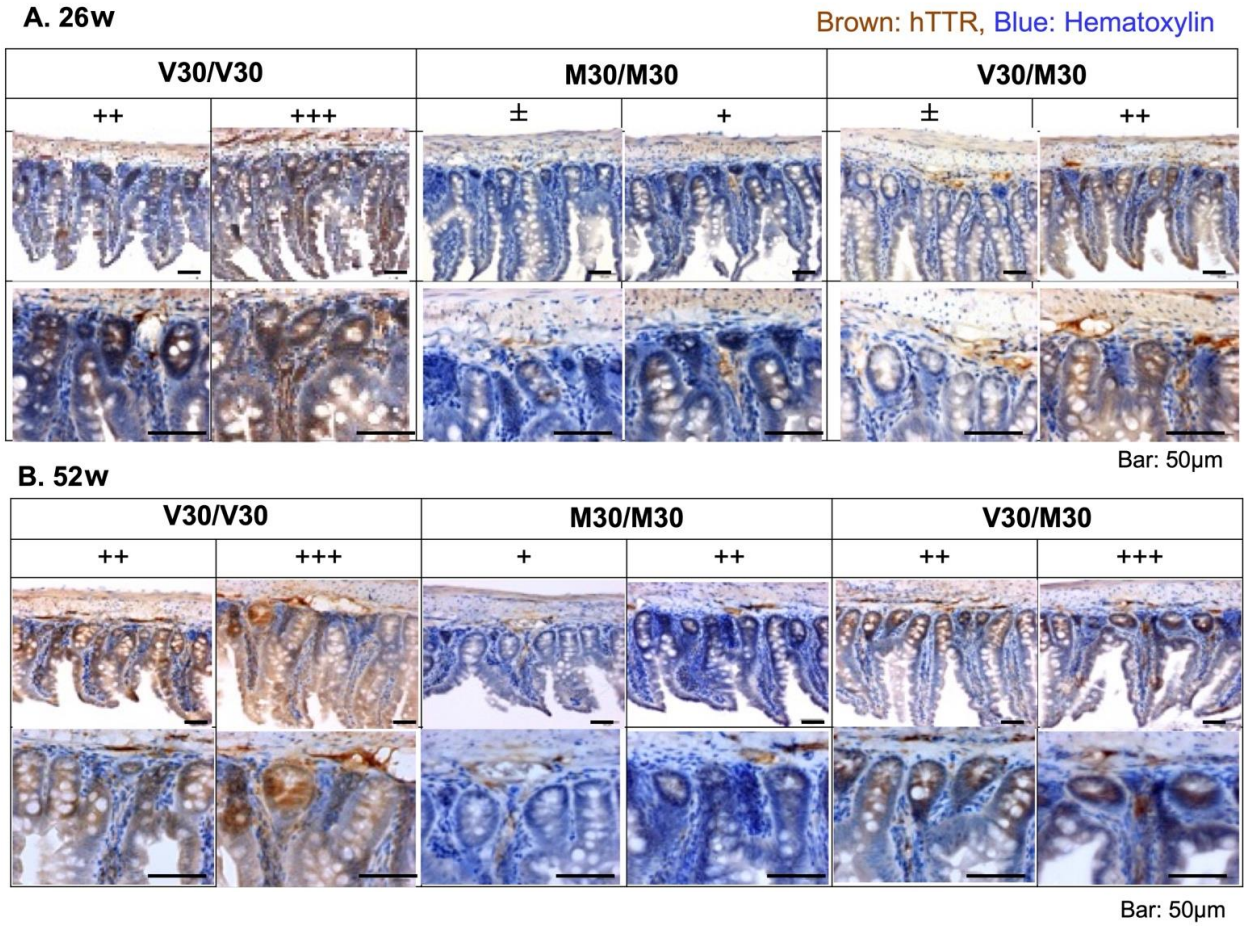

Figure 5: Representative Immunohistochemical Staining of hTTR Deposition in ileum

Representative anti-human TTR immunohistochemical staining images of ileum from V30/V30, M30/M30, and V30/M30 mice at 26 and 52 weeks of age are shown. V30/V30 and V30/M30 mice showed extensive hTTR-positive staining, whereas M30/M30 mice showed limited deposition.

3.6. Genotype-Dependent hTTR Deposition in Kidney

In kidney, TTR deposition also differed markedly among genotypes. At 26 weeks of age, V30/V30 mice showed maximal or near-maximal staining, M30/M30 mice showed minimal staining, and V30/M30 mice showed strong staining. The mean deposition scores were 3.00 ± 0.00 in V30/V30 mice, 0.50 ± 0.00 in M30/M30 mice, and 2.60 ± 0.24 in V30/M30 mice. The genotype effect was significant, and pairwise comparisons showed that M30/M30 mice had significantly lower scores than both V30/V30 and V30/M30 mice. At 52 weeks of age, kidney deposition showed an even clearer genotype-dependent pattern. V30/V30 and V30/M30 mice showed maximal deposition scores in all animals, whereas M30/M30 mice retained low scores. The mean scores were 3.00 ± 0.00 in V30/V30 mice, 0.70 ± 0.12 in M30/M30 mice, and 3.00 ± 0.00 in V30/M30 mice. Pairwise comparisons again showed significantly lower deposition in M30/M30 mice than in the other two genotypes. These findings demonstrate that kidney TTR deposition is strongly genotype-dependent and that M30/M30 mice are relatively resistant to TTR deposition despite carrying the Met30 allele homozygously.

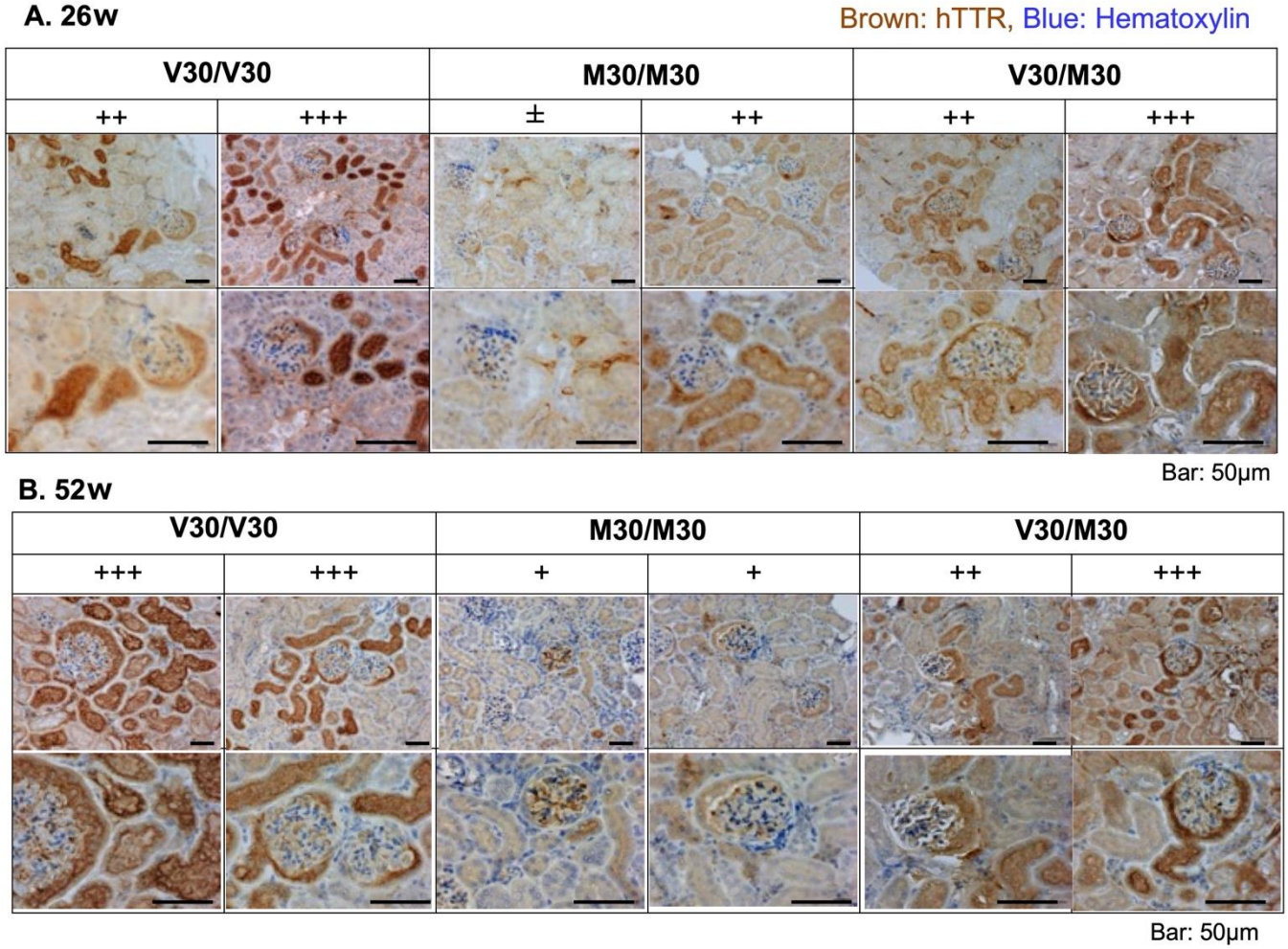

Figure 6: Representative Immunohistochemical Staining of hTTR Deposition in Kidney

Representative anti-human TTR immunohistochemical staining images of kidney from V30/V30, M30/M30, and V30/M30 mice at 26 and 52 weeks of age are shown. Strong hTTR-positive signals were observed in V30/V30 and V30/M30 mice, particularly in glomeruli and proximal tubules, whereas M30/M30 mice showed minimal staining.

3.7. hTTR Deposition in Sciatic Nerve

At 52 weeks of age, TTR-positive deposits were detected in the sciatic nerve. Although the overall amount of deposition was lower than that observed in ileum and kidney, detectable staining in sciatic nerve is notable because peripheral nerve deposition is rarely observed in mouse models of TTR amyloidosis. The mean sciatic nerve deposition scores were 2.20 ± 0.37 in V30/V30 mice,

0.60 ± 0.10 in M30/M30 mice, and 0.80 ± 0.12 in V30/M30 mice. The genotype effect was significant. Pairwise comparisons showed that V30/V30 mice had significantly higher deposition scores than M30/M30 mice, and V30/V30 mice tended to show higher scores than V30/M30 mice. No significant difference was observed between M30/M30 and V30/M30 mice. These results indicate that TTR exon-humanized mice can develop detectable TTR deposition in peripheral nerve tissue. The sciatic nerve deposition pattern differed somewhat from that observed in ileum and kidney, suggesting tissue-specific factors in TTR deposition.

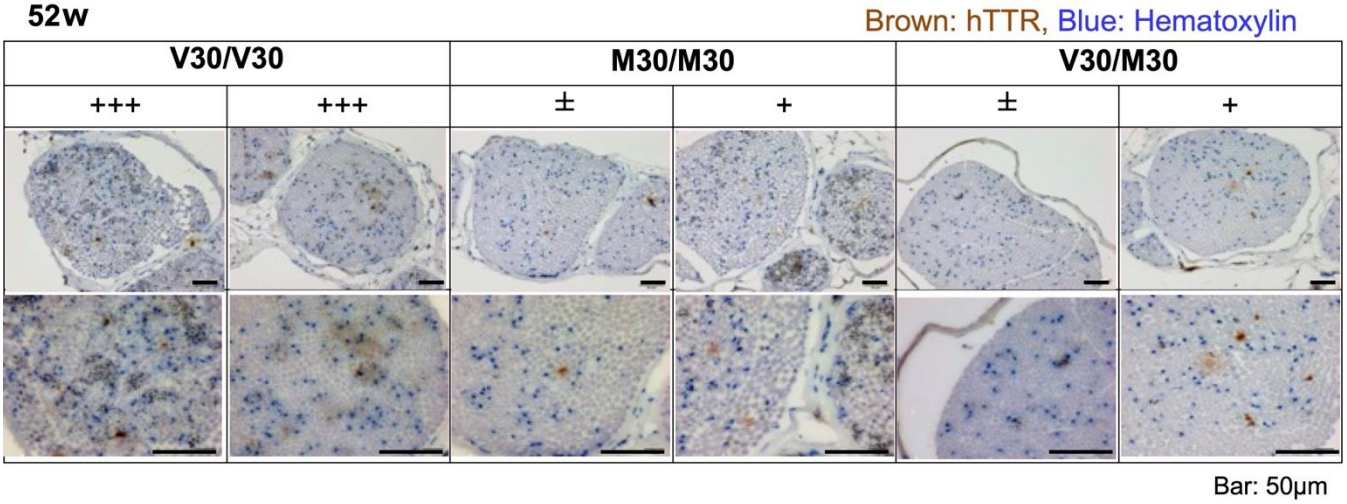

Figure 7: Representative Immunohistochemical Staining of hTTR deposition in sciatic nerve

Representative anti-human TTR immunohistochemical staining images of sciatic nerve at 52 weeks of age are shown. hTTR-positive deposits were detected in sciatic nerve, particularly in V30/V30 mice. Although the overall amount of deposition was lower than in ileum and kidney, detectable TTR deposition in sciatic nerve indicates the utility of this model for studying peripheral nerve involvement.

3.8. Direct Fast Scarlet Staining did not Detect Amyloid Fibrils

To determine whether the TTR-positive deposits represented mature amyloid fibrils, Direct fast scarlet staining was performed. Although immunohistochemistry revealed substantial hTTR deposition, Direct fast scarlet staining did not detect definitive amyloid fibril deposition corresponding to the hTTR-positive areas. Under polarized light, no convincing amyloid-specific birefringence was observed in the TTR-positive deposits. These findings indicate that the TTR deposits observed in this study are most likely non-fibrillar TTR deposits or pre-amyloid deposits rather than mature amyloid fibrils. This distinction is important because anti-TTR antibody-positive deposits may represent an early stage of TTR deposition preceding amyloid fibril formation.

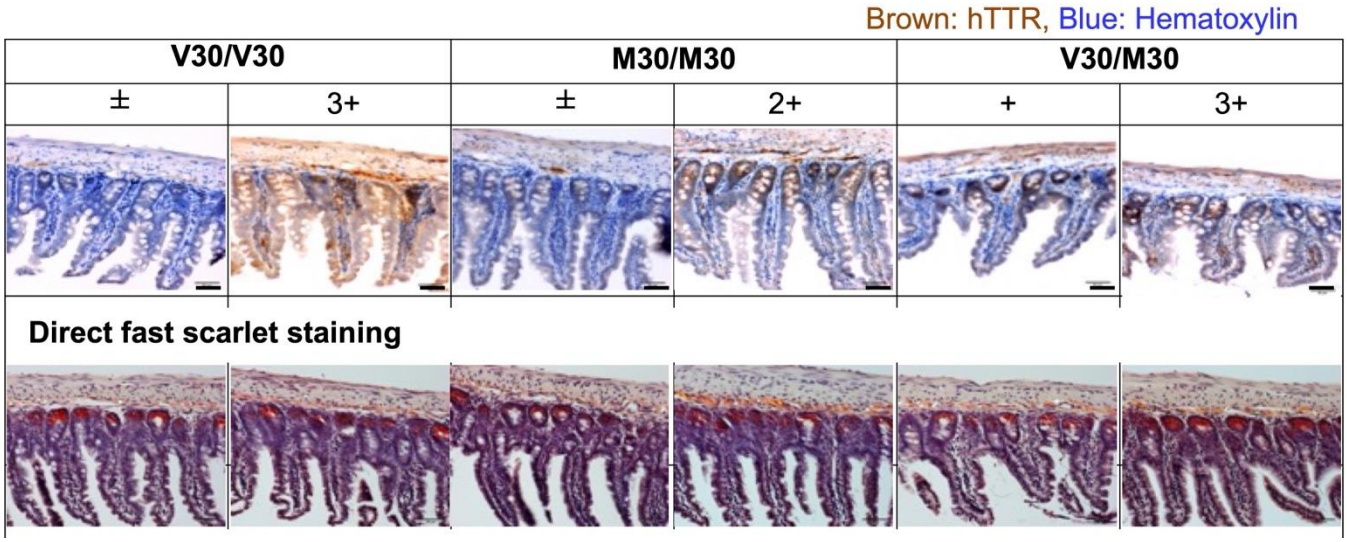

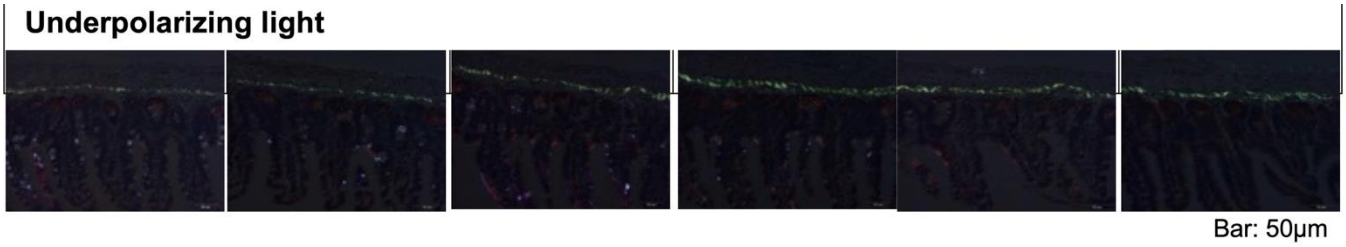

Figure 8: Direct Fast Scarlet Staining for Amyloid Fibril Deposition

Direct fast scarlet staining was performed to detect amyloid fibrils. Although anti-human TTR immunohistochemistry revealed hTTR-positive deposits, Direct fast scarlet staining did not detect definitive amyloid fibrils corresponding to the hTTR-positive deposits. These findings suggest that the deposits are non-fibrillar or pre-amyloid TTR deposits.

3.9. Serum hTTR Levels

Serum human TTR levels were measured in V30/V30, M30/M30, and V30/M30 mice. At the analyzed ages, serum hTTR levels showed modest genotype-dependent differences (Figure 10A). The overall differences in serum hTTR were smaller than those observed for TTR deposition. These results suggest that tissue deposition in this model is not explained solely by serum hTTR concentration.

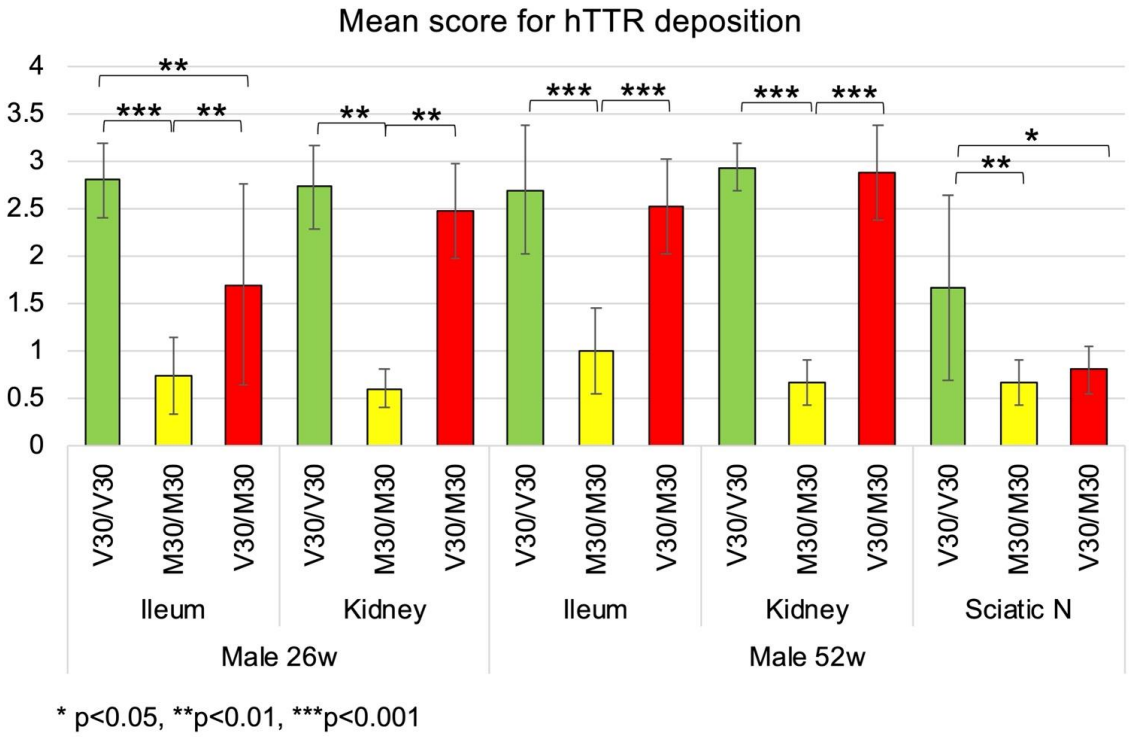

Figure 9: Semi-Quantitative Analysis of non-fibrillar hTTR Deposition in Various Genotypes

Mean hTTR deposition scores are shown for ileum and kidney at 26 and 52 weeks of age and for sciatic nerve at 52 weeks of age. TTR deposition differed significantly among genotypes. M30/M30 mice showed lower deposition scores than V30/V30 and V30/M30 mice in ileum and kidney.

3.10. Serum mRBP4 Levels

Serum mouse RBP4 levels differed markedly among genotypes. Serum mRBP4 levels were highest in wild-type control mice, lower in M30/M30 mice, and lowest in V30/V30 mice. Thus, the order of serum mRBP4 levels was: wild-type control > M30/M30 > V30/V30.

This pattern suggests that the serum concentration of RBP4 may be strongly influenced by its interaction with TTR. Because non-TTR-bound RBP4 is expected to undergo glomerular filtration and urinary loss, reduced TTR-RBP4 binding stability may result in decreased circulating RBP4 levels.

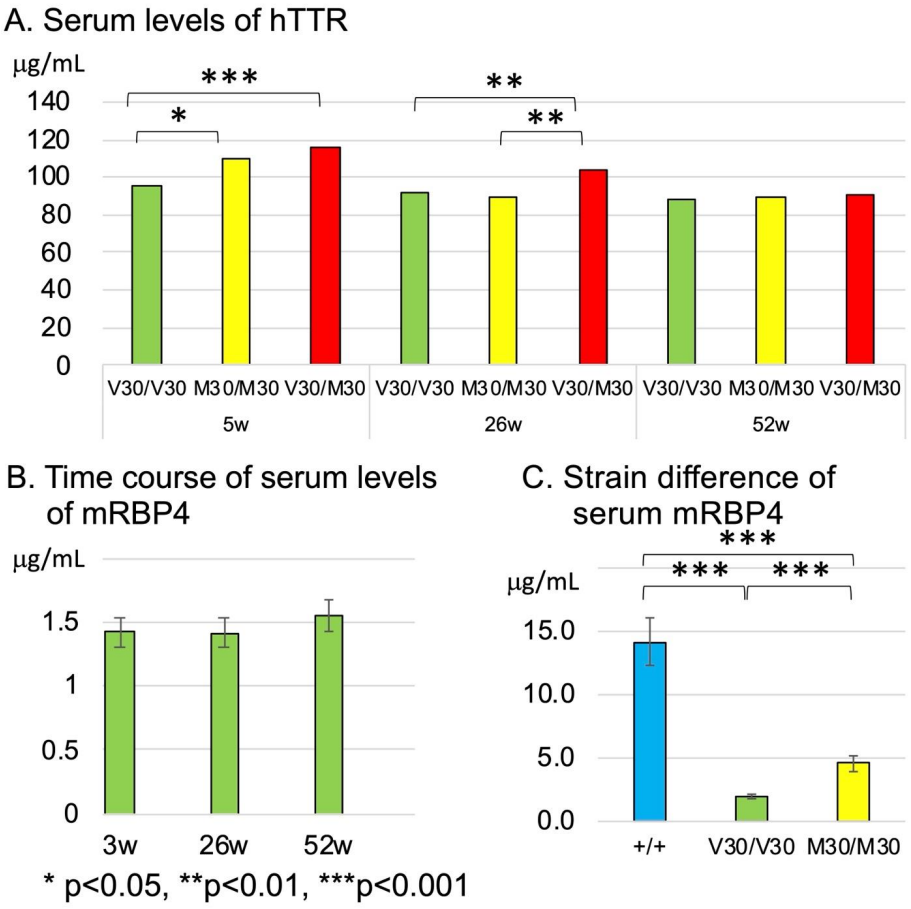

Figure 10: Serum hTTR and mRBP4 levels in various genotypes

A, Serum hTTR levels in V30/V30, M30/M30, and V30/M30 mice. n=15 males. B, Time course of serum mRBP4 levels. n=10 males. C, Strain differences in serum mRBP4 levels. n=10 males. Serum mRBP4 levels were highest in wild-type control mice, lower in M30/M30 mice, and lowest in V30/V30 mice.

time \ TTR		mTTR4	hTTRWild	hTTRV30M
5000ps	chain B	−68.01	−46.4	−43.3
	chain C	−50.68	−38.35	−51.32
6300ps	chain B	−70.46	−45.39	−43.93
	chain C	−50.34	−38.70	−50.17
7500ps	chain B	−72.29	−44.39	−46.37
	chain C	−50.1	−38.75	−50.33
8800ps	chain B	−73.41	−42.43	−48.89
	chain C	−49.95	−39.82	−50.35
10000ps	chain B	−74.44	−37.4	−50.22
	chain C	−49.65	−39.26	−50.16
mean±sd		−60.93±10.91	−41.09±3.11	−48.5±2.75

[kcal/mol]

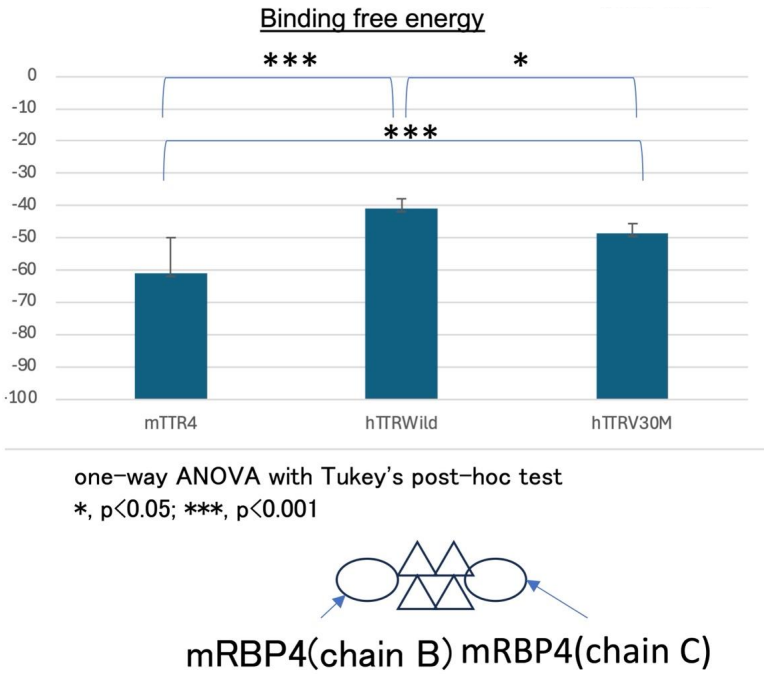

Figure 11: Supportive Computational Analysis of TTR-RBP4 Binding Stability

Binding free energy between each TTR tetramer and mouse RBP4-retinol was calculated using gmx_MMPBSA after molecular dynamics-based structural refinement. More negative values indicate more stable binding. The calculated binding free energy was most negative for mouse TTR-mouse RBP4-retinol, intermediate for human TTR Val30Met-mouse RBP4-retinol, and least negative for human TTR Val30-mouse RBP4-retinol. These data support the possibility that genotype-dependent differences in TTR-RBP4 binding stability contribute to the observed differences in serum RBP4 levels.

3.11. Supportive Computational Analysis of TTR-RBP4 Binding Stability

To obtain supportive mechanistic information on the relationship between TTR genotype and serum RBP4 levels, we performed computational analysis of the binding stability between TTR tetramers and mouse RBP4-retinol. Binding free energy was calculated using gmx_MMPBSA after molecular dynamics-based structural refinement. The calculated binding free energy was most negative for the mouse TTR–mouse RBP4-retinol complex, intermediate for the human TTR Val30Met–mouse RBP4-retinol complex, and least negative for the human wild-type TTR Val30–mouse RBP4-retinol complex. The calculated values were −60.93 ± 10.91 kcal/mol for mouse TTR, −48.50 ± 2.75 kcal/mol for human TTR Val30Met, and −41.09 ± 3.11 kcal/mol for human wild-type TTR Val30. Because more negative binding free energy values indicate more stable binding, the predicted order of TTR-RBP4 binding stability was: mouse TTR > human TTR Val30Met > human TTR Val30. This predicted order was consistent with the serum mRBP4 levels, which were highest in wild-type mice, relatively preserved in M30/M30 mice, and lowest in V30/V30 mice. These findings support the possibility that genotype-dependent differences in TTR-RBP4 binding stability contribute to the observed differences in serum RBP4 levels and tissue TTR deposition.

4. Discussion

In the present study, we generated TTR exon-humanized mice carrying the Val30Met mutation and analyzed genotype-dependent TTR deposition in V30/V30, M30/M30, and V30/M30 mice. The major findings are as follows. First, anti-human TTR-positive deposits were detected in multiple tissues, including ileum, kidney, and sciatic nerve. Second, TTR deposition could be evaluated semi-quantitatively using tissue-specific pathological scoring criteria. Third, TTR deposition was genotype-dependent, with M30/M30 mice consistently showing lower deposition than V30/V30 and V30/M30 mice in ileum and kidney. Fourth, TTR-positive deposits were detected in the sciatic nerve at 52 weeks of age. Fifth, Direct fast scarlet staining did not detect mature amyloid fibrils, suggesting that the observed deposits represent non-fibrillar or pre-amyloid TTR deposition. Finally, serum mRBP4 levels and supportive computer simulation analysis were consistent with the possibility that RBP4 stabilizes circulating TTR in a genotype-dependent manner. The present model differs from conventional TTR transgenic mouse models in several important ways. In transgenic models, human TTR expression is often driven by exogenous promoter elements and may be influenced by transgene copy number and insertion site. In addition, endogenous mouse TTR remains present in many models, allowing formation of mouse-human hybrid tetramers. Such hybrid tetramers are more stable than human TTR homotetramers and may interfere with amyloidogenesis. By contrast, the TTR exon-humanized model

preserves the mouse genomic structure and regulatory context while replacing the coding exons with human TTR exons. This design allows human TTR protein to be expressed under the control of the endogenous Ttr locus. Therefore, TTR exon-humanized mice provide a physiologically relevant platform for analyzing human TTR biology in vivo.

A key feature of the present study is the semi-quantitative evaluation of TTR deposition. Previous studies of TTR deposition in mouse models [7,14,18,19] often reported the number of animals with positive deposits in each tissue. Although such information is useful, it does not fully capture the degree or distribution of deposition. In the present study, anti-human TTR immunohistochemistry revealed unexpectedly broad and frequent TTR-positive deposits. Therefore, we established tissue-specific scoring criteria and converted staining intensity and distribution into numerical scores. This approach allowed statistical comparison of deposition among genotypes, tissues, and ages. The scoring system revealed a clear genotype-dependent pattern, particularly in ileum and kidney.

One unexpected finding was that M30/M30 mice showed lower TTR deposition than V30/V30 and V30/M30 mice. At first glance, this may appear paradoxical because the Met30 variant is associated with hereditary amyloid polyneuropathy in humans. However, most patients with Val30Met-associated amyloidosis are heterozygous, and homozygous Val30Met patients are rare and not necessarily more severely affected. The present data suggest that the heterozygous state, or the coexistence of Val30 and Met30 TTR subunits, may create a molecular environment more favorable for TTR deposition than the Met30 homozygous state. In this regard, the present model may provide a useful experimental system for investigating why heterozygous Val30Met is clinically important and why homozygous Val30Met is not simply a more severe version of the disease.

The detection of TTR-positive deposits in the sciatic nerve is also important. Peripheral nerve involvement is a defining feature of hereditary TTR amyloidosis in humans, but peripheral nerve deposition has been difficult to reproduce in mouse models. In previous studies, amyloid deposition in the sciatic nerve was rare and often required additional genetic or environmental factors [14,18]. In the present study, TTR-positive deposits were detected in the sciatic nerve of exon-humanized mice at 52 weeks of age. Although the amount of deposition was lower than in ileum and kidney, this finding indicates that the model can reproduce at least part of the peripheral nerve deposition process. Interestingly, the genotype-dependent pattern in sciatic nerve differed from that in ileum and kidney, suggesting that local tissue factors may influence TTR deposition.

Direct fast scarlet staining did not detect mature amyloid fibrils despite the presence of abundant anti-human TTR-positive deposits. This indicates that the observed TTR deposits are likely non-fibrillar or pre-amyloid deposits. This distinction is biologically important. TTR amyloidogenesis is thought to proceed from tetramer dissociation to monomer misfolding, non-fibrillar aggregation, protofibril formation, and mature amyloid fibril deposition. Anti-TTR-positive, Direct fast scarlet-negative deposits may therefore represent an early stage of tissue deposition, consistent with previous reports of non-fibrillar TTR deposits [18,19]. The present model may be particularly useful for studying early events in TTR deposition before the formation of mature amyloid fibrils. The relationship between serum hTTR concentration and tissue deposition was not straightforward. Although serum hTTR levels showed some genotype-dependent differences, these differences were not sufficient to explain the striking differences in tissue deposition. This suggests that qualitative factors, such as tetramer stability, TTR-RBP4 interaction, and tissue microenvironment, may be more important than total serum hTTR concentration alone.

The serum mRBP4 data provide an important clue. RBP4 circulates in plasma primarily as a complex with TTR. When RBP4 is not bound to TTR, it is more readily filtered by the kidney and lost from the circulation. Therefore, serum RBP4 levels may reflect the stability of the TTR–RBP4 complex. In the present study, serum mRBP4 levels were markedly lower in V30/V30 mice and relatively preserved in M30/M30 mice. The supportive computational analysis further strengthens the possible link between TTR-RBP4 interaction and the in vivo findings. Using an updated molecular dynamics-based workflow and gmx_MMPBSA binding free-energy calculation, the predicted binding stability between TTR and mouse RBP4-retinol was highest for mouse TTR, intermediate for human TTR Val30Met, and lowest for human wild-type TTR Val30. This order paralleled the serum mRBP4 levels observed in vivo.

Because RBP4 is retained in the circulation through its interaction with TTR, reduced binding stability between TTR and RBP4 may lead to decreased circulating RBP4. Conversely, weaker TTR-RBP4 interaction may increase the fraction of unbound or less stabilized TTR, potentially facilitating tissue deposition. Thus, although the computational analysis was not intended as primary evidence, it provides supportive mechanistic data consistent with the hypothesis that RBP4 functions as an endogenous stabilizing partner for circulating TTR.

Several limitations should be noted. First, the TTR deposition score is semi-quantitative and based on pathological assessment rather than fully automated image analysis. However, because deposition patterns differed among tissues and were widely distributed, simple area-based quantification was not appropriate. Second, Direct fast scarlet staining did not detect amyloid fibrils, so the present findings primarily reflect non-fibrillar or pre-amyloid TTR deposition. Third, these computational data should be interpreted together with the pathological and biochemical findings rather than as independent proof of binding behavior in vivo. Fourth, RBP4 data were not available for all genotype and age combinations. Further biochemical analyses, including direct assessment of TTR–RBP4 complexes in serum, would strengthen the mechanistic interpretation. Despite these limitations, the present study demonstrates that TTR exon-humanized mice are a

valuable model for analyzing genotype-dependent TTR deposition. The model preserves the endogenous genomic context, allows comparison of clinically relevant genotypes, and reveals tissue-specific deposition patterns including sciatic nerve involvement. Furthermore, the integration of tissue deposition, serum RBP4 levels, and supportive simulation analysis suggests that RBP4 may play an important stabilizing role in TTR biology.

In conclusion, TTR exon-humanized mice carrying Val30 and Met30 alleles reveal genotype-dependent non-fibrillar TTR deposition in multiple tissues. M30/M30 mice show unexpectedly low deposition compared with V30/V30 and V30/M30 mice, suggesting that TTR deposition is not determined simply by the presence of the Met30 allele. The detection of TTR deposition in sciatic nerve further supports the utility of this model for studying human TTR amyloidosis. These findings establish TTR exon-humanized mice as a useful model for investigating early TTR deposition and provide supportive evidence that RBP4 functions as a natural stabilizer of circulating TTR.

Author Contributions

K.Y. developed the research concept and wrote the manuscript.
Z.L. performed genetic experiments.
H.K. performed gene editing experiments.
Y.M. performed biochemical and pathological analyses.
T.T.,N.M. and R.F. performed animal care and genetic manipulation.
Z.L., A.S., M.O., and Y.T. performed formal analysis.
Z.L. edited the manuscript.
All authors approved the final manuscript.

Funding

This research received no external funding.

Competing Interests

The authors declare no competing interests.

Declaration of generative AI and AI-assisted technologies in the manuscript preparation process

During the preparation of this work, the authors used ChatGPT (OpenAI) to assist with English language editing and refinement of manuscript wording. After using this tool, the authors reviewed and edited the content as needed and take full responsibility for the content of the published article.

References

1. Andrade, C. (1952). A peculiar form of peripheral neuropathy: familiar atypical generalized amyloidosis with special involvement of the peripheral nerves. *Brain, 75*(3), 408-427.
2. Dwulet, F. E., & Benson, M. D. (1984). Primary structure of an amyloid prealbumin and its plasma precursor in a heredofamilial polyneuropathy of Swedish origin. *Proceedings of the National Academy of Sciences, 81*(3), 694-698.
3. Tawara, S., Nakazato, M., Kangawa, K., Matsuo, H., & Araki, S. (1983). Identification of amyloid prealbumin variant in familial amyloidotic polyneuropathy (Japanese type). *Biochemical and biophysical research communications, 116*(3), 880-888.
4. Colon, W., & Kelly, J. W. (1992). Partial denaturation of transthyretin is sufficient for amyloid fibril formation in vitro. *Biochemistry, 31*(36), 8654-8660.
5. Lai, Z., Colón, W., & Kelly, J. W. (1996). The acid-mediated denaturation pathway of transthyretin yields a conformational intermediate that can self-assemble into amyloid. *Biochemistry, 35*(20), 6470-6482.
6. Reixach, N., Foss, T. R., Santelli, E., Pascual, J., Kelly, J. W., & Buxbaum, J. N. (2008). Human-murine transthyretin heterotetramers are kinetically stable and non-amyloidogenic: a lesson in the generation of transgenic models of diseases involving oligomeric proteins. *Journal of Biological Chemistry, 283*(4), 2098-2107.
7. Tagoe, C. E., Tagoe, C. E., Reixach, N., Tagoe, C. E., Reixach, N., Friske, L., ... & Buxbaum, J. N. (2007). In vivo stabilization of mutant human transthyretin in transgenic mice. *Amyloid, 14*(3), 227-236.
8. Takahashi, K., Watanabe, S., Murakami, T., Ikegawa, S., Araki, S., Yamarnura, K. I., & Yi, S. (1994). Systemic amyloidosis in transgenic mice carrying the human mutant transthyretin (Met 30) gene. *Molecular Neurobiology, 8*, 15-23.
9. Takaoka, Y., Tashiro, F., Yi, S., Maeda, S., Shimada, K., Takahashi, K., ... & Yamamura, K. I. (1997). Comparison of amyloid deposition in two lines of transgenic mouse that model familial amyloidotic polyneuropathy, type I. *Transgenic research, 6*(4), 261-269.
10. Takaoka, Y., Ohta, M., Miyakawa, K., Nakamura, O., Suzuki, M., Takahashi, K., ... & Sakaki, Y. (2004). Cysteine 10 is a key residue in amyloidogenesis of human transthyretin Val30Met. *The American journal of pathology, 164*(1), 337-345.
11. Inoue, S., Ohta, M., Li, Z., Zhao, G., Takaoka, Y., Sakashita, N., ... & Yamamura, K. I. (2008). Specific pathogen free conditions prevent transthyretin amyloidosis in mouse models. *Transgenic research, 17*(5), 817-826.
12. Zhao, G., Li, Z., Araki, K., Haruna, K., Yamaguchi, K., Araki, M., ... & Yamamura, K. I. (2008). Inconsistency between hepatic expression and serum concentration of transthyretin in mice humanized at the transthyretin locus. *Genes to Cells, 13*(12), 1257-1268.
13. Liu, L., Suzuki, T., Shen, J., Wakana, S., Araki, K., Yamamura, K. I., ... & Li, Z. (2017). Rescue of retinal morphology and function in a humanized mouse at the mouse retinol-binding protein locus. *Laboratory Investigation, 97*(4), 395-408.
14. Li, X., Lyu, Y., Shen, J., Mu, Y., Qiang, L., Liu, L., ... & Li, Z. (2018). Amyloid deposition in a mouse model humanized at the transthyretin and retinol-binding protein 4 loci. *Laboratory Investigation, 98*(4), 512-524.
15. Li, Z., Kanazashi, H., Tokashiki, Y., Fujikawa, R., Okagaki, A., Katoh, S., ... & Yamamura, K. (2022). TTR exon-humanized mouse optimal for verifying new therapies for FAP. *Biochemical and biophysical research communications, 599*, 69-74.
16. White, J. T., & Kelly, J. W. (2001). Support for the multigenic hypothesis of amyloidosis: the binding stoichiometry of retinol-binding protein, vitamin A, and thyroid hormone influences

transthyretin amyloidogenicity in vitro. *Proceedings of the National Academy of Sciences, 98*(23), 13019-13024.

17. Zanotti, G., & Berni, R. (2004). Plasma retinol-binding protein: structure and interactions with retinol, retinoids, and transthyretin. *Vitamins and hormones, 69*, 271-295.
18. Sousa, M. M., Fernandes, R., Palha, J. A., Taboada, A., Vieira, P., & Saraiva, M. J. (2002). Evidence for early cytotoxic aggregates in transgenic mice for human transthyretin Leu55Pro. *The American journal of pathology, 161*(5), 1935-1948.
19. Teng, M. H., Yin, J. Y., Vidal, R., Ghiso, J., Kumar, A., Rabenou, R., ... & Buxbaum, J. (2001). Amyloid and nonfibrillar deposits in mice transgenic for wild-type human transthyretin: a possible model for senile systemic amyloidosis. *Laboratory investigation, 81*(3), 385-396.